© 2018. Published by The Company of Biologists Ltd | Journal of Cell Science (2018) 131, jcs209924. doi:10.1242/jcs.209924

RESEARCH ARTICLE

Unconventional myosin VIIA promotes melanoma progression

Yuqing Liu[1,2,*], Xiaofan Wei[1,*], Lizhao Guan[1], Sidi Xu[1], Yang Yuan[1], Danyu Lv[1], Xiaokun He[1], Jun Zhan[1], Yan Kong[3], Jun Guo[3] and Hongquan Zhang[1,‡]

ABSTRACT

Unconventional myosin VIIA (Myo7a) is an actin-based motor molecule that normally functions in the cochlear hair cells of the inner ear. Mutations of *MYO7A*/*Myo7a* have been implicated in inherited deafness in both humans and mice. However, there is limited information about the functions of Myo7a outside of the specialized cells of the ears. Herein, we report a previously unidentified function of Myo7a by demonstrating that it plays an important role in melanoma progression. We found that silencing *Myo7a* by means of RNAi inhibited melanoma cell growth through upregulation of cell cycle regulator p21 (also known as CDKN1A) and suppressed melanoma cell migration and invasion through downregulation of RhoGDI2 (also known as ARHGDIB) and MMP9. Furthermore, Myo7a depletion suppressed melanoma cell metastases to the lung, kidney and bone in mice. In contrast, overexpression of Myo7a promoted melanoma xenograft growth and lung metastasis. Importantly, Myo7a levels are remarkably elevated in human melanoma patients. Collectively, we demonstrated for the first time that Myo7a is able to function in non-specialized cells, a finding that reveals the complicated disease-related roles of Myo7a, especially in melanomas.

KEY WORDS: Unconventional Myo7a, Melanoma, Tumor metastasis, RhoGDI2

INTRODUCTION

Melanoma is characterized by its increasing incidence, aggressive clinical behavior and propensity for lethal metastasis (Jemal et al., 2013; Marsh Durban et al., 2013). However, the mechanisms underlying these properties remain elusive. Unconventional myosins are a superfamily of actin-based motor proteins and have vital roles in numerous cellular processes, including intracellular transport, organization of F-actin, mitotic spindle regulation and gene transcription (Berg et al., 2001; Foth et al., 2006; Richards and Cavalier-Smith, 2005; Woolner and Bement, 2009). Myosins consist of three distinct regions, a head, neck and tail. The heads are motor domains that are homologous among different myosins, whereas the tails display diversity and have combinations of a variety of functional domains, which determine the individual cellular functions (Hirano et al., 2011).

Myosin VIIA (Myo7a) is an unconventional myosin closely associated with inherited hearing loss. Previous studies have suggested that Myo7a is mainly expressed in the stereocilia of inner ear hair cells, and is essential for maintenance of the staircase-like bundle and the resting tension (Frolenkov et al., 2004; Kros et al., 2002; Rzadzinska et al., 2009). Mutations in *MYO7A* cause syndromic (USH1B) (Weil et al., 1995) and non-syndromic (DFNB2 and DFNA11) (Liu et al., 1997a,b; Tamagawa et al., 2002; Weil et al., 1997) deafness in humans. Mutations in *Myo7a* are also responsible for recessive deafness in shaker-1 mice (Gibson et al., 1995; Mburu et al., 1997). In addition, Myo7a is expressed in the photoreceptor and retinal pigment epithelial cells of the retina, participating in opsin transport (Liu et al., 1999), melanosome transport along the apical processes (Futter, 2006; Futter et al., 2004; Lopes et al., 2007) and the phagocytosis of retinal pigment epithelial cells to the rod outer segments shed from photoreceptor cells (Soni et al., 2005). Most of studies have been focused on the roles of Myo7a in auditory and visual processes, whereas little is known about its functions in other systems, including cancer.

Structurally, the tail of Myo7a contains two protein 4.1, ezrin, radixin, moesin (FERM) domains. Many FERM-containing proteins play important roles in tumor development. Some of these inhibit tumor motility, such as FRMD5 (Wang et al., 2012), while others promote tumor progression such as ERM proteins (Gautreau et al., 2002). Our previous studies have demonstrated that the Myo10 FERM domain interacts with an NPXY motif that is located within the β-integrin cytoplasmic domain, and silencing of Myo10 through siRNA impaired integrin function in cell adhesion (Zhang et al., 2004). Another study has reported that mutant p53-associated Myo10 upregulation promotes breast cancer invasion and metastasis (Arjonen et al., 2014). As Myo7a contains FERM domains, we propose that Myo7a may play an important role in tumor progression. Notably, it has been reported that *MYO7A* variant S1666C (rs2276288) is associated with increased risk of malignant melanoma in a case-control study, suggesting that Myo7a might play important roles in melanoma development (Fernandez et al., 2009). Importantly, our previous study demonstrated that Myo7a interacts with integrin β5 and selectively promotes integrin αvβ5-mediated cell adhesion and migration (Liu et al., 2014). These findings imply that the biological functions of Myo7a are related to tumor progression. However, few reports have identified the biological functions of Myo7a, or the relationship between Myo7a and tumor progression. In the present study, we demonstrated that Myo7a promotes melanoma cell growth, cell migration and tumor metastasis. We further investigated the underlying molecular mechanisms of the role of Myo7a in melanoma progression.

[1]Laboratory of Molecular Cell Biology and Tumor Biology, Department of Anatomy, Histology and Embryology, Key Laboratory of Carcinogenesis and Translational Research, Ministry of Education, and State Key Laboratory of Natural and Biomimetic Drugs, Peking University Health Science Center, Beijing 100191, China. [2]Department of Molecular Neuropathology, Beijing Neurosurgical Institute and Chinese Glioma Cooperative Group (CGCG), Capital Medical University, Beijing 100050, China. [3]Key Laboratory of Carcinogenesis and Translational Research (Ministry of Education), Department of Renal Cancer and Melanoma, Peking University Cancer Hospital and Institute, Beijing 100142, People's Republic of China.
*These authors contributed equally to this work

‡Author for correspondence (Hongquan.Zhang@bjmu.edu.cn)

H.Z., 0000-0003-1088-9862

Received 18 August 2017; Accepted 11 January 2018

Journal of Cell Science (2018) 131, jcs209924. doi:10.1242/jcs.209924

RESULTS

Myo7a is highly expressed in mouse B16 melanoma cells

To explore the biological functions of Myo7a in tumors, we had previously detected the expression of Myo7a in various tumor cell lines, including B16, MCF-7, MDA-MB-231, H1299, SW480 and HeLa cells, and our results showed that B16 is the only cell line that endogenously expresses high levels of Myo7a (see supplementary data Fig. 1B in Liu et al., 2014). Therefore, B16 cells can be used for the loss of function study of Myo7a. Next, we assessed the expression of Myo7a in seven human melanoma cell lines; the results revealed that Myo7a was weakly expressed in A375 and WM983a cells, whereas it was undetectable in other cells (Fig. 1A). Moreover, *Myo7a* mRNA levels were measured and the results also showed high expression of *Myo7a* in B16 cells and weak expression in A375 and WM983a cells (Fig. 1B). Two *Myo7a*-specific siRNAs were synthesized, and these significantly inhibited the protein expression of endogenous Myo7a in B16 cells (Fig. 1C). To explore the functional role of Myo7a in melanoma cells, a B16 cell line with stable knockdown of Myo7a (Fig. 1D) and an A375 cell line stably overexpressing Myo7a (Fig. 1E) were established.

Myo7a promotes melanoma cell proliferation and tumor growth

First, we examined the effects of Myo7a on proliferation of melanoma cells. The results showed that knockdown of Myo7a significantly inhibited the proliferation of B16 cells *in vitro* (Fig. 2A). By the fifth day, the absorbance of *Myo7a* shRNA-transfected B16 cells was nearly half of that in control cells (Fig. 2B). Next, a soft agar colony formation assay, the results of which are considered to closely relate to the level of *in vivo* tumorigenicity, was performed to assess the anchorage-independent growth of B16 cells. Compared to control cells, fewer colonies were observed in Myo7a knockdown B16 cells (Fig. 2C,D), which suggests that knockdown of Myo7a strongly inhibited the colony formation of B16 cells. To further identify the roles of Myo7a in melanoma cell proliferation *in vivo*, xenograft models were established to determine the contribution of Myo7a to tumor growth. In this experiment, six C57BL/6 mice were inoculated with B16 *Myo7a* shRNA and B16 control shRNA cells at different sides on the back, and the tumors were visualized after 2 weeks. Consistent with *in vitro* studies, Myo7a knockdown B16 cells grew more slowly than control cells *in vivo* (Fig. 2E,F), and the tumor mass was also significantly lower in mice inoculated with Myo7a knockdown B16 cells (Fig. 2G). On the other hand, Myo7a-overexpressing A375 cells had a greater tumorigenic ability than control cells (Fig. 2H,I), and tumor masses exhibited the same tendency (Fig. 2J). Taken together, these results suggest that Myo7a promotes tumor growth both *in vitro* and *in vivo*.

Myo7a promotes tumor cell migration and invasion

Myo7a is a motor protein that has been shown to regulate cellular movement, and, in our previous study, we found that Myo7a promoted integrin αvβ5-mediated cell migration (Liu et al., 2014). Thus we sought to further confirm the effects of Myo7a on melanoma cell mobility. To verify this, confluent and quiescent monolayers of B16 cells transfected with *Myo7a* shRNA and control shRNA were scratched and cell mobility was observed at different time points (0, 6 and 16 h). The results

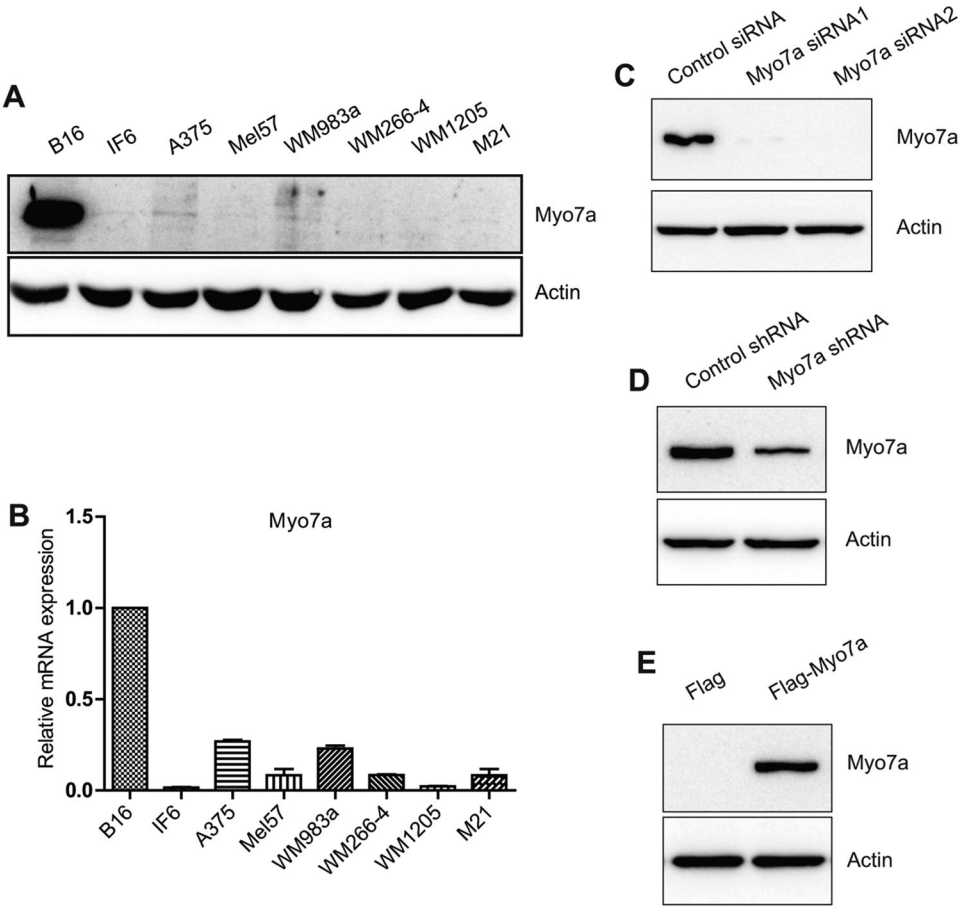

Fig. 1. Myo7a is highly expressed in B16 mouse melanoma cells. (A) The expression profile of Myo7a in seven human melanoma cell lines was examined by western blot analyses using an anti-Myo7a polyclonal antibody. B16 cell lysate was used as positive control and results show that human melanoma A375 cell line expresses low level of Myo7a. (B) The expression of Myo7a was determined by qPCR in B16 cells and seven human melanoma cell lines. (C) The knockdown efficiency of two Myo7a siRNAs was examined in B16 mouse melanoma cells. (D) B16 mouse melanoma cells stably expressing Myo7a shRNA were established and examined by western blot analysis. (E) A375 cells stably expressing Flag–Myo7a were established and examined by western blot analysis using an anti-Myo7a polyclonal antibody.

Journal of Cell Science (2018) 131, jcs209924. doi:10.1242/jcs.209924

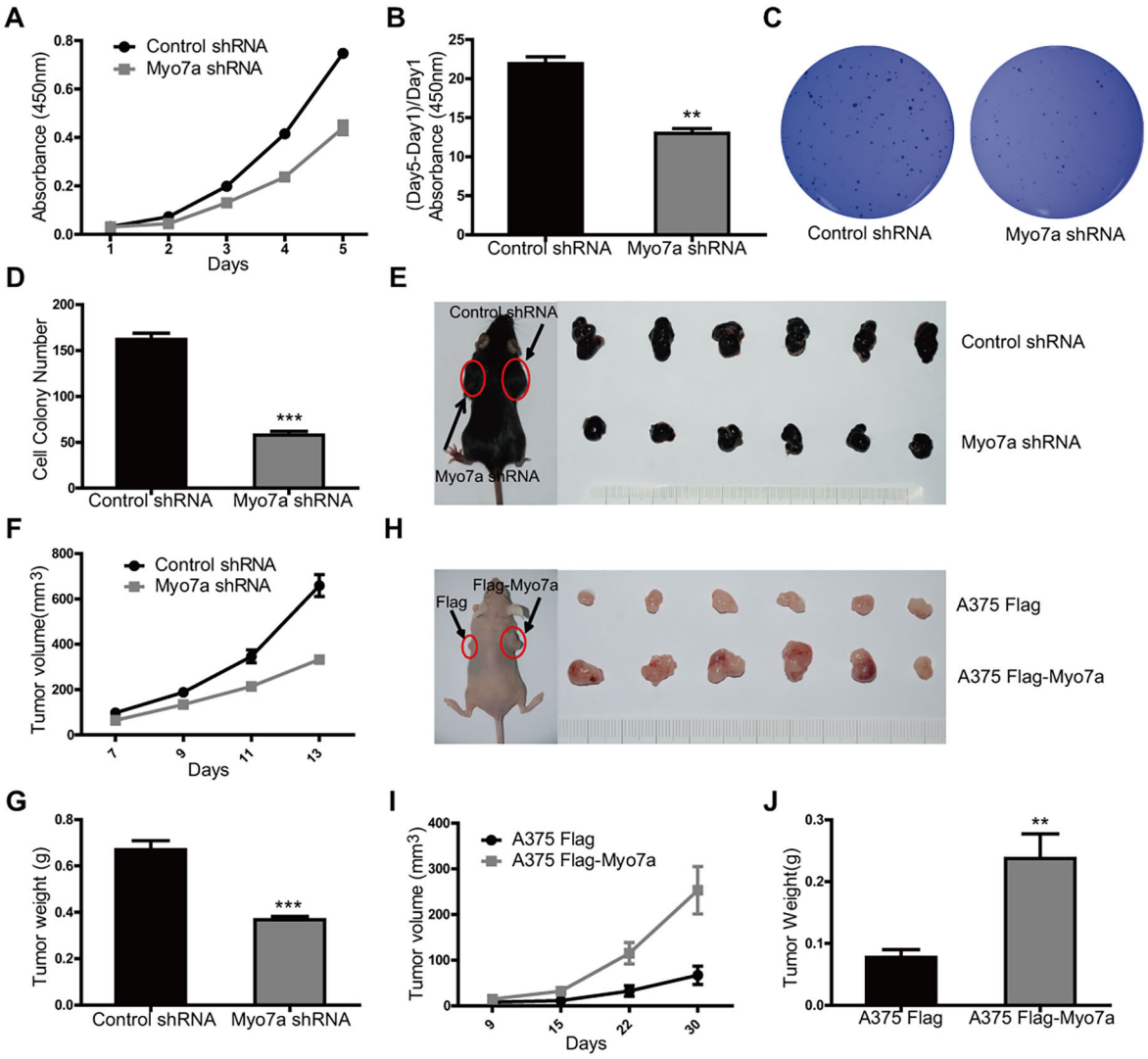

Fig. 2. Myo7a promotes cell proliferation *in vitro* and *in vivo*. (A) Stable knockdown of Myo7a inhibits B16 cell proliferation. B16 cells with stable knockdown of endogenous Myo7a were cultured for the indicated number of days and cell viability was then determined by means of the WST-1 assay. (B) Quantitative analysis of cell proliferation. The vertical ordinate shows the ratio of the difference between the optical density (OD; absorbance at 450 nm) value at day 5 and day 1 compared to the basal OD value. Data are expressed as means±s.d.; n=3 independent experiments (**P<0.01). (C) Myo7a knockdown suppresses colony formation in a soft agar assay. (D) Quantification of the colony formation in soft agar. Data are expressed as means±s.d.; n=3 independent experiments (***P<0.001). (E) Knockdown of Myo7a inhibited B16 tumor growth *in vivo*. The left panel shows one representative C57BL/6 mouse that was injected with the indicated cells on both sides of the mouse back. The right panel shows the tumors resected from six mice. (F) Tumors in the Myo7a knockdown group grew more slowly than those in the control group. The difference between the two groups was clearly seen on day 11. (G) The tumor weight in mouse was decreased in the Myo7a knockdown group. Data are expressed as means±s.d.; n=3 independent experiments (**P<0.01). (H) Overexpression of Myo7a in A375 human melanoma cells promoted tumor growth in the nude mice. (I) Tumors in the Myo7a overexpression group grew faster than that in the control group. (J) The tumor weight was increased in the Myo7a overexpression group. Data are expressed as means±s.d.; n=3 independent experiments (***P<0.001).

showed that knockdown of Myo7a diminished the rate of wound closure in B16 cells (Fig. 3A), indicating that Myo7a promoted lateral cell migration. In addition, we observed random cell motility of B16 cells, as monitored by time-lapse confocal microscopy. Cell tracking of ten B16 cells selected randomly is presented in Fig. 3B. Cell tracking of another 20 B16 cells in each group is shown in Fig. S1. Similarly, the results showed that knockdown of Myo7a in B16 cells greatly reduced both cell migration velocity and total cell migration distance (Fig. 3C,D). Moreover, Transwell migration assays were performed to uncover the effects of Myo7a on vertical migration of tumor cells. The results revealed that knockdown of Myo7a suppressed the vertical migration of B16 tumor cells (Fig. 3E), while overexpression of Myo7a greatly promoted the migration of A375 cells (Fig. 3G). Moreover, *in vitro* invasion assays were performed to investigate the effects of Myo7a on tumor cell invasion. As shown in Fig. 3F, Myo7a knockdown cells displayed a significantly decreased ability to invade through a Matrigel-coated chamber, in comparison to control cells. Consistent with the above results, overexpression of Myo7a obviously promoted invasion by A375 cells (Fig. 3H). Taken together, these results indicate that Myo7a promotes melanoma cell migration and invasion *in vitro*.

Myo7a regulates tumor metastasis

To further validate the above results, we investigated the effects of Myo7a on melanoma metastasis *in vivo* through tail vein injection of B6 cells with stable knockdown of Myo7a. At 14 days after injection,

Journal of Cell Science (2018) 131, jcs209924. doi:10.1242/jcs.209924

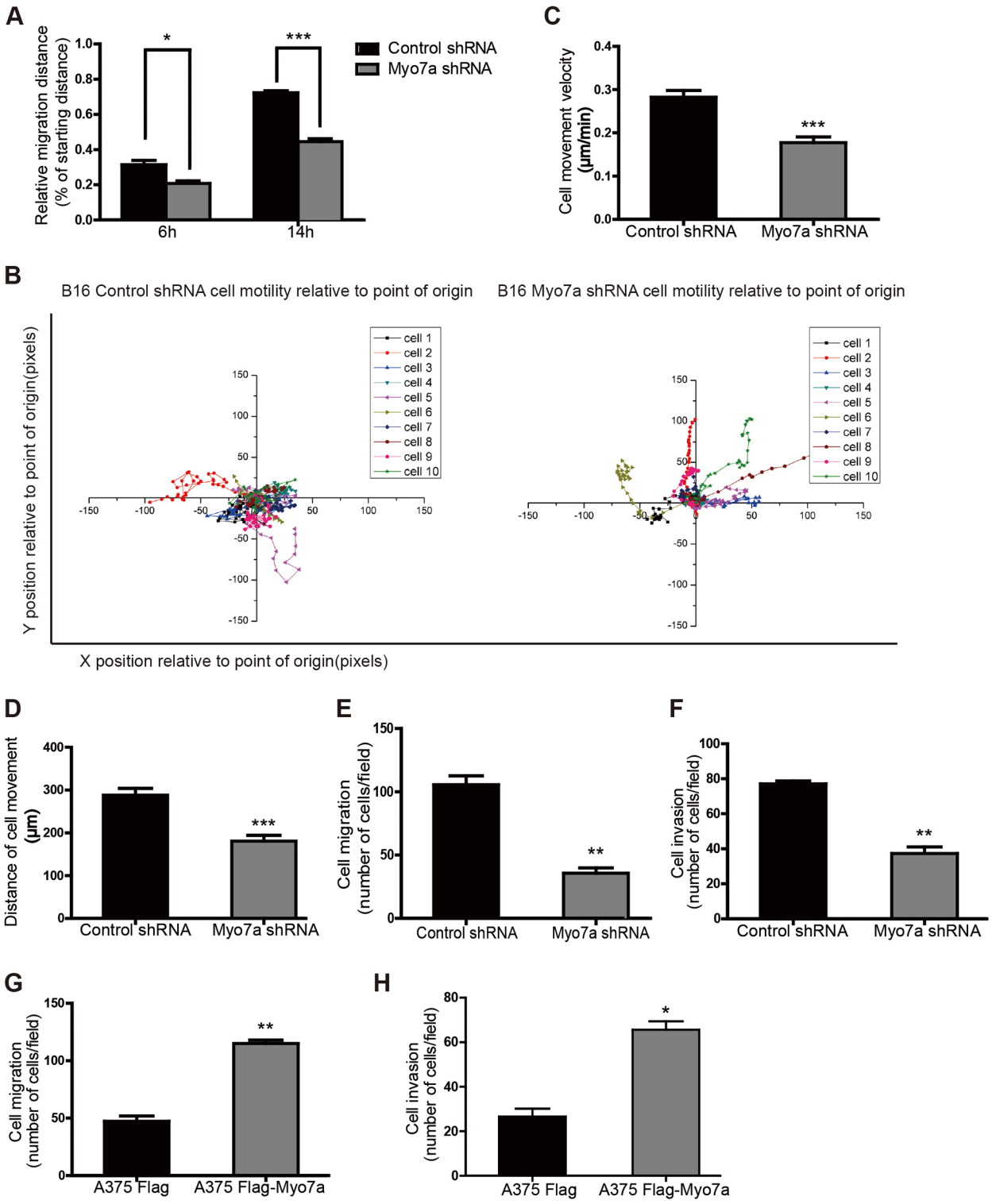

Fig. 3. Myo7a promotes tumor cell migration and invasion. (A) Knockdown of Myo7a inhibits B16 cell migration in a cell wound healing assay. Data were expressed as means±s.d.; *n*=3 independent experiments (6 h: **P*<0.05; 14 h: ****P*<0.001). (B) Analyses of random cell motility via video microscopy showed that the cell movement velocity (C) and distance (D) are significantly decreased in Myo7a knockdown cells. Data are expressed as means±s.d.; *n*=3 independent experiments (****P*<0.001). (E,F). *In vitro* migration and invasion assays of Myo7a knockdown cells or control cells, respectively. Data are expressed as means±s.d.; *n*=3 independent experiments (***P*<0.01). (G,H) Overexpression of Myo7a promoted cell migration and invasion in A375 cells. Data are expressed as means±s.d.; *n*=3 independent experiments (***P*<0.01; **P*<0.05).

mice were killed, and then several organs including lungs and kidneys were removed and fixed. Representative pictures of lungs from each group are shown in Fig. 4A. A drastic reduction in melanoma nodules was found in the lungs of the Myo7a knockdown group, as compared to what was found for the control group. Consistently, the weight of the lungs from treated mice was significantly lower than in controls

Journal of Cell Science (2018) 131, jcs209924. doi:10.1242/jcs.209924

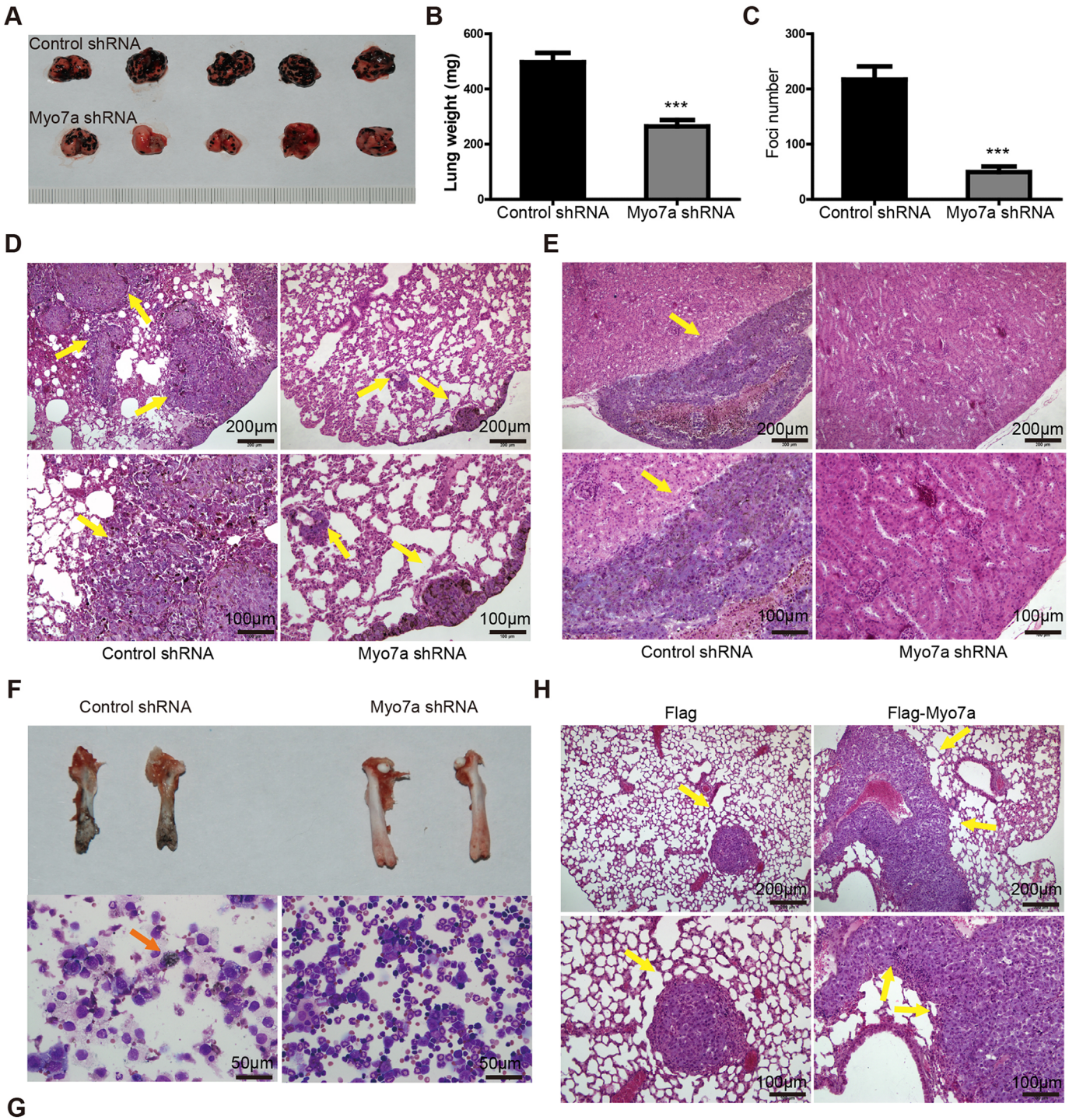

G

	Proportion of kidney with melanoma nodules	Proportion of femur with melanoma nodules
Control shRNA	8/10	7/10
Myo7a shRNA	0/10	0/10

Fig. 4. Myo7a regulates tumor metastasis. (A) Images of lungs from each group show considerably less metastatic foci in mice treated with Myo7a shRNA-transfected B16 cells, compared to controls, which was also evidenced by their significantly lower weight (***P<0.001) (B). (C,D) Foci counting and representative images of histological examination (D, yellow arrowheads) revealed less and smaller nodules in the group treated with Myo7a shRNA-transfected B16 cells than in controls (***P<0.001). (E) Representative images of H&E-stained kidney metastasis showed that metastatic foci only exist in the treatment group. (F) Knockdown of Myo7a inhibited bone metastasis. The upper panels show two pairs of representative femurs. The lower panels show the bone marrow smear. The orange arrow indicates the metastatic tumor cell. (G) Number of kidneys and femurs with melanoma cell islands over the number examined. Five pairs of kidneys and femurs in each group were examined. (H) Overexpression of Myo7a promoted lung metastasis of A375 cells. H&E staining shows more significant metastasis in Myo7a overexpressing tumor (arrows).

(Fig. 4B). Furthermore, there were significantly fewer metastatic foci in lung tissue treated with *Myo7a* shRNA than in the control groups and these foci were also smaller (Fig. 4C). H&E staining also revealed a high density of tumor nodules that had invaded most of the lung parenchyma in the control group, but many fewer tumor nodules in the Myo7a knockdown group (Fig. 4D). Furthermore, kidney metastasis was only observed in control group animals, which was confirmed by H&E staining (Fig. 4E,G). Surprisingly, there was femur metastasis in control cells, and bone marrow smears revealed melanoma cells scattered among bone marrow blasts, which were not observed in mice injected with *Myo7a* shRNA transfected cells (Fig. 4F,G). Moreover, H&E staining of the lung tissue sections also showed broader areas of tumors for mice with Myo7a overexpressing cells (Fig. 4H). These data indicate that Myo7a regulates melanoma cell metastasis to the lung and bone.

Knockdown of Myo7a induces G1 arrest by regulating the expression of p21 and Cdk2

To elucidate the molecular mechanisms through which Myo7a is involved in the proliferation and metastasis of melanoma cells, we performed high-throughput RNA sequencing (RNA-seq) to analyze the transcriptomes of B16 cells transfected with *Myo7a* shRNA versus those of the control group. The list of 1348 differentially expressed genes between the two groups can be found as Table S1, and a heat map showed 140 genes [those with reads per kilobase million (RPKM) values greater than 1 and values of $\log_2$ (fold change) greater than 1.5 or less than −1.5] among them, including genes of interest (Fig. 5A). Some of these genes encode proteins associated with cell cycle and tumor metastasis, such as p21 (also called Cdkn1a), Cdk2 and MMP9. Next, real-time quantitative PCR (RT-qPCR) was used to validate the RNA-seq results. Indeed, knockdown of Myo7a increased the expression of p21 and inhibited the expression of Cdk2 at the transcriptional level, and the expression of MMP9 was also significantly diminished in Myo7a knockdown cells (Fig. 5B), an observation further supported by western blots (Fig. 5C). We also found that overexpression of Myo7a downregulated p21 expression in A375 cells (Fig. S2). It is known that p21, a cyclin-dependent kinase inhibitor, plays a critical role in the regulation of the G1 to S phase transition during the cell cycle. To determine whether knockdown of Myo7a inhibited cell proliferation of melanoma cells through blocking the G1-S transition, a flow cytometry cell cycle analysis was performed. The results showed that knockdown of Myo7a caused a significant increase in the G1 population and a decrease in the S population in B16 cells (Fig. 5D,E). In contrast, Myo7a overexpression led to a decrease of the G1 population and an increase in the S population in A375 cells (Fig. 5F; Fig. S3). To determine whether p21 is required for the Myo7a knockdown-mediated cell cycle inhibition, p21 was knocked down by means of siRNA in B16 *Myo7a* shRNA cells and in control B16 cells (Fig. 5G). As expected, p21 knockdown partially rescued the cell cycle arrest induced by Myo7a knockdown, whereas no obvious changes were observed in control cells (Fig. 5H). Representative FACS results are shown in Fig. S3. Collectively, these data indicate that knockdown of Myo7a induced G1 arrest by upregulating the expression of p21 and inhibiting the expression of its downstream protein Cdk2.

Myo7a regulates cell motility via RhoGDI2 and activated Rac1

To explore the molecular mechanisms of Myo7a-regulated tumor cell motility, two-dimensional gel electrophoresis following mass spectrometry was used to isolate proteins differentially expressed between B16 *Myo7a* shRNA cells and control cells. Five protein spots were found to be differentially expressed between the two groups (Fig. 6A; Fig. S4). Among the five protein spots, we found that Rho GDP-dissociation inhibitor 2 (RhoGDI2; also known as ARHGDIB), which promotes the activation of Rho GTPases essential for cell motility, was downregulated in B16 *Myo7a* knockdown cells (Fig. 6A). We then validated the expression of RhoGDI2 protein by means of western blotting (Fig. 6B). Our results also showed that overexpression of Myo7a upregulated RhoGDI2 expression in A375 cells (Fig. S2). Moreover, knockdown of Myo7a led to reduction of the mRNA level of *RhoGDI2*, which is consistent with the data from RNA-seq (Fig. 6C). Knockdown of RhoGDI2 efficiently reduced cell migration ability in B16 cells (Fig. 6D,E). To determine whether RhoGDI2 is required for Myo7a-induced cell motility, a Flag-tagged RhoGDI2 expression vector or empty vector was transfected into B16 *Myo7a* shRNA cells and into control cells, respectively (Fig. 6F). Overexpressed RhoGDI2 promoted cell migration and rescued the inhibition of cell motility caused by knockdown of Myo7a (Fig. 6G). Next, we tested the activities of the endogenous Rho GTPases in B16 cells by performing a GST pulldown assay. The results showed that knockdown of Myo7a resulted in a significant decrease in Rac1 activity (Fig. 6H). However, there was no obvious difference in the activity of Cdc42 between the control cells and *Myo7a* shRNA-transfected cells. On the other hand, Rac1 activity was significantly elevated when Flag-tagged RhoGDI2 was transfected into B16 *Myo7a* shRNA cells and into control cells. In summary, the above results suggest that Myo7a promotes the invasiveness of melanoma cells partially by regulating RhoGDI2 expression and the activity of Rac1.

Enhanced Myo7a expression was observed in human melanoma

Given that Myo7a regulates melanoma progression in cells and mouse xenografts, as shown above, we speculated whether Myo7a expression is increased in human melanoma. To this end, we examined Myo7a levels by immunohistochemical staining in both normal and tumor tissues of melanoma patients (n=15). We found that Myo7a expression was greatly increased in the melanoma tissues of 11 patients compared to normal tissues. Results from three patients are shown in Fig. 7A. Other results are provided in Fig. S5. Furthermore, upregulated expression levels of Myo7a in melanoma were confirmed also seen in the Oncomine data bank (https://www.oncomine.org/) (Fig. 7B). These results further indicate that Myo7a plays an important role in the regulation of melanoma progression.

DISCUSSION

Myo7a was initially identified as the gene defective in shaker-1 mice and in human USH1B (Gibson et al., 1995; Weil et al., 1995). Although Myo7a has been extensively studied since then, our knowledge of mammalian Myo7a is still limited to its functions in auditory and visual processes. No studies have characterized the effects of Myo7a in tumor progression. In this study, we demonstrated for the first time that Myo7a plays important roles in regulating the cell proliferation, motility, invasion and metastasis of melanoma cells. Importantly, we found that Myo7a expression is significantly upregulated in human melanomas.

Previous studies have shown that Myo7a is expressed in cells with cilia or microvilli, such as hair cells, retinal pigment epithelium (RPE) cells, kidney tubules, lung bronchi and in Sertoli cells of the testis (Wolfrum et al., 1998). The expression of Myo7a in normal skin melanocytes has not been reported, and Myo7a was undetectable in rat skin (Hasson et al., 1995). In our study, we

Journal of Cell Science (2018) 131, jcs209924. doi:10.1242/jcs.209924

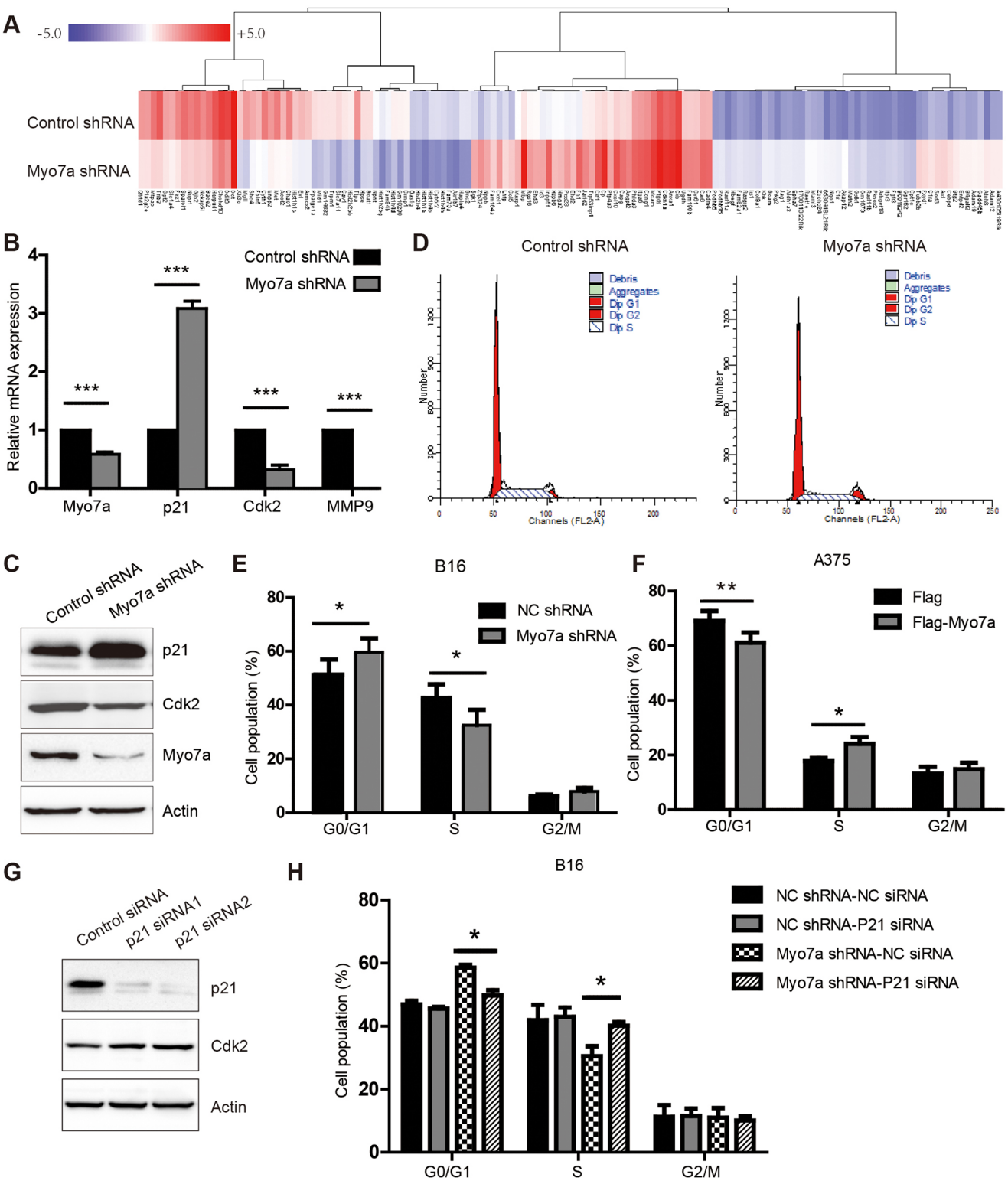

Fig. 5. Knockdown of Myo7a induces G1 arrest by regulating the expression of p21 and Cdk2. (A) The heatmap indicates differentially expressed genes between B16-Myo7a shRNA cells and the control cells. The color of blue and red represents the relative expression of genes. The darker the red is, the greater the gene expression. The darker the blue is, the lower the gene expression. The lines indicate various clusters have similar metrics as based on the Pearson correlation. (B) The expression of p21, Cdk2 and MMP9 was determined by qPCR in Myo7a shRNA cells and the control cells. Data were expressed as means± s.d.; n=3 independent experiments (***P<0.001). (C) The expression of p21 and Cdk2 was determined by western blotting using the indicated antibodies in Myo7a shRNA cells and the control cells. (D,E) Cell cycle analysis of Myo7a shRNA cells and the control cells (D), and quantitative analysis of FACS (E). Dip in D means diploid. Data are expressed as means±s.d. from three independent experiments (B16: *P<0.05). (F) Quantitative cell cycle analysis for A375 cells overexpressing Myo7a and control cells. Data are expressed as means±s.d.; n=3 independent experiments (A375: **P<0.01). (G) Knockdown of p21 by two specific siRNAs upregulated the protein level of Cdk2 in B16 cells as determined by western blotting using indicated antibodies. (H) Quantitative analysis of cell cycle in B16 Myo7a shRNA cells and the control cells treated with siRNA targeted p21 and control siRNA, respectively.

Journal of Cell Science (2018) 131, jcs209924. doi:10.1242/jcs.209924

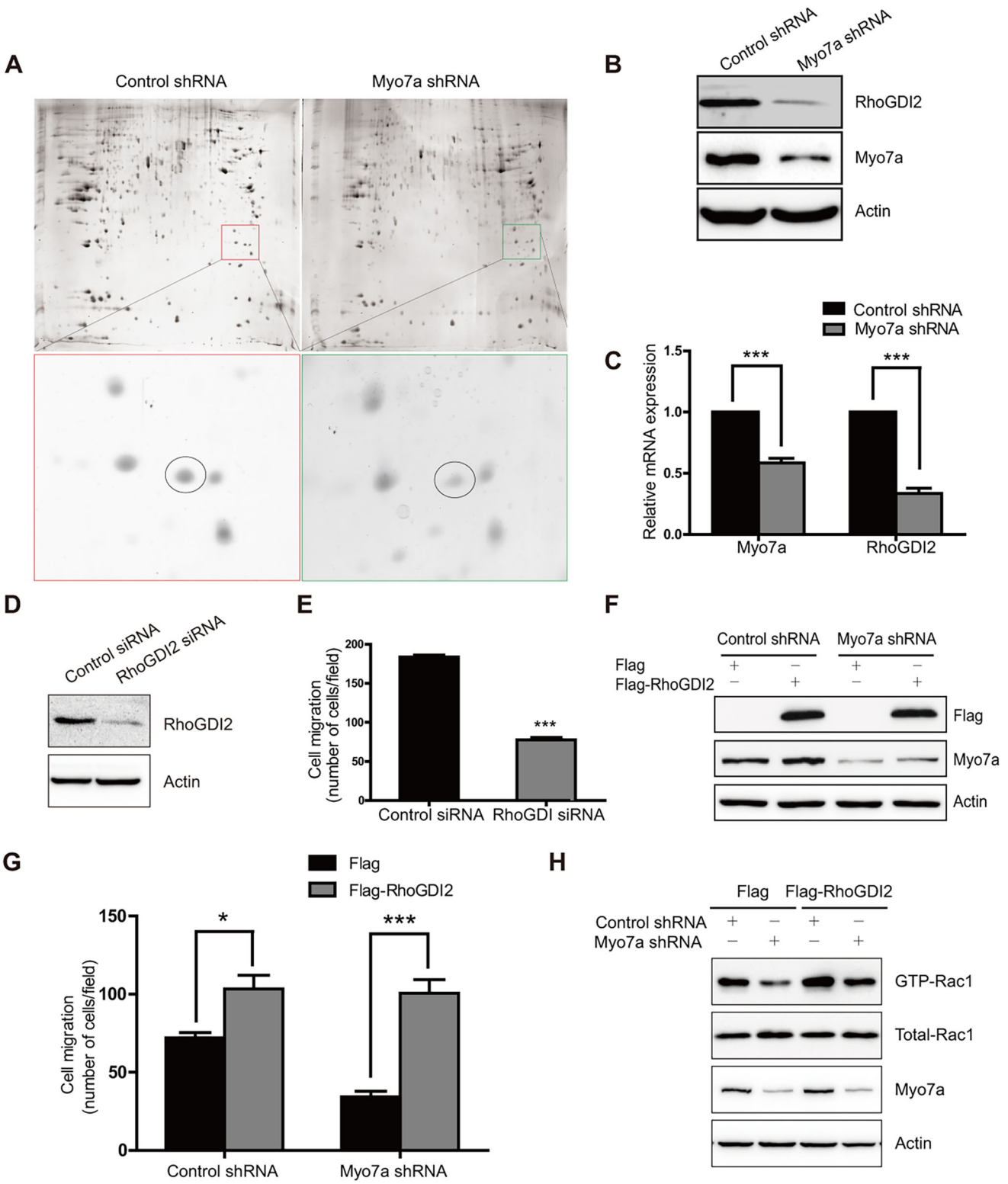

Fig. 6. Myo7a regulates tumor cell motility via RhoGDI2 and activated Rac1. (A–C) Differential expression of RhoGDI2 in B16-Myo7a shRNA cells and the control cells was identified by 2D-electrophoresis. The upper panels showed the whole images of cellular proteins from B16-Myo7a shRNA cells and the control cells. The lower panels are a magnified view of the boxes in the upper panels, in which the RhoGDI2 spots are circled (A). The expression of RhoGDI2 was reduced in Myo7a shRNA cells compared to the control cells as determined by western blotting (B) and also by qPCR (C). Data are expressed as means±s.d.; n=3 independent experiments (***P<0.001). (D) The knockdown efficiency of RhoGDI2 siRNA in B16 cells. (E) Knockdown of RhoGDI2 inhibited B16 cell migration as determined by a Transwell migration assay. Data are expressed as means±s.d.; n=3 independent experiments (***P<0.001). (F) The transfection efficiency of Flag–RhoGDI2 or empty vector in B16-Myo7a knockdown cells and the control cells was determined by western blotting using an anti-Flag antibody. (G) Transiently overexpressed RhoGDI2 rescued the reduced cell motility in Myo7a shRNA cells as determined by a Transwell migration assay. Data are expressed as means±s.d.; n=3 independent experiments (control shRNA: *P<0.05; Myo7a shRNA: ***P<0.001). (H) Myo7a knockdown led to reduced activation of Rac1 that could be rescued partially by RhoGDI2 in B16 cells.

Journal of Cell Science (2018) 131, jcs209924. doi:10.1242/jcs.209924

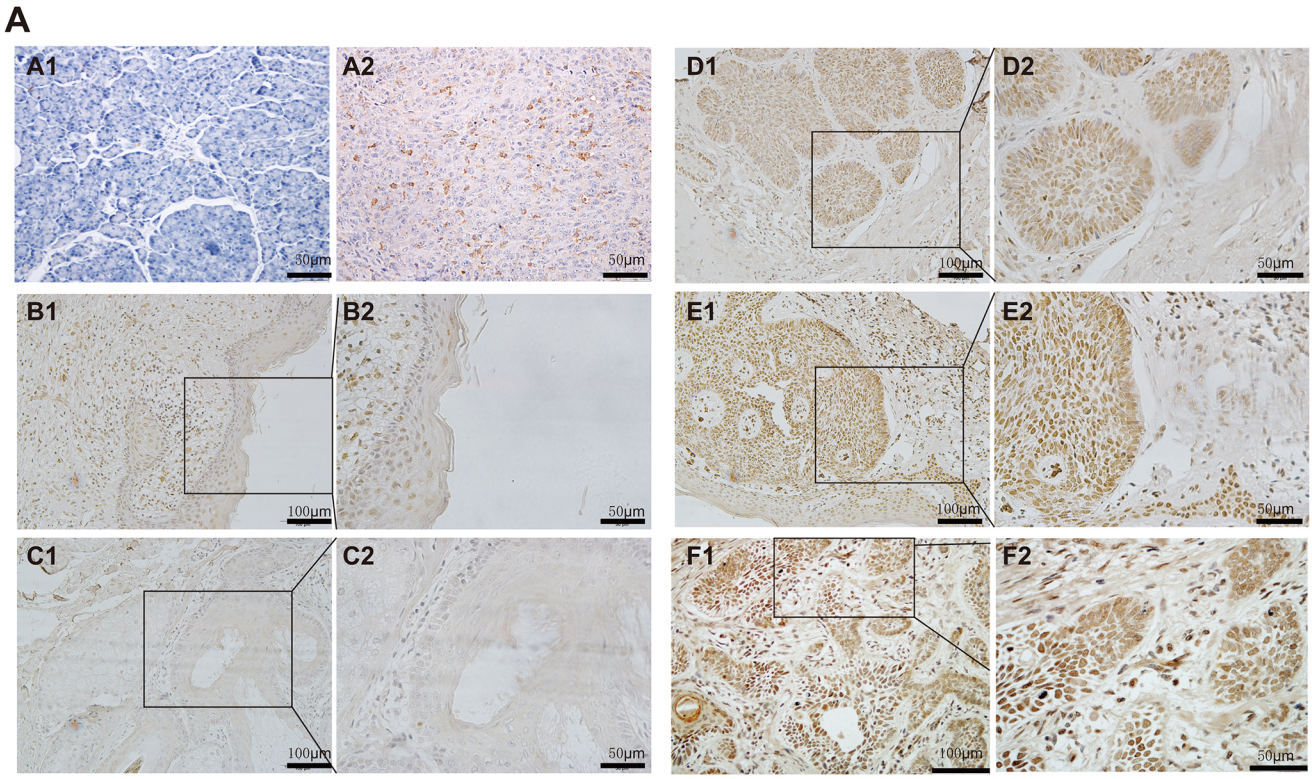

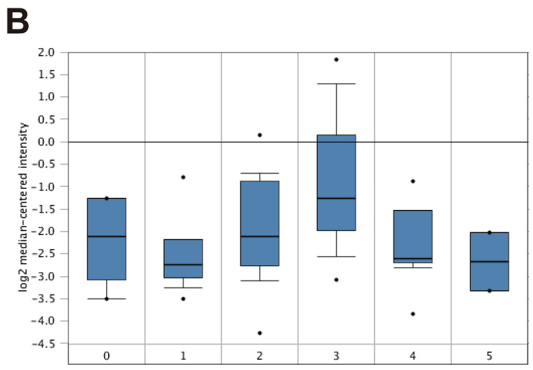

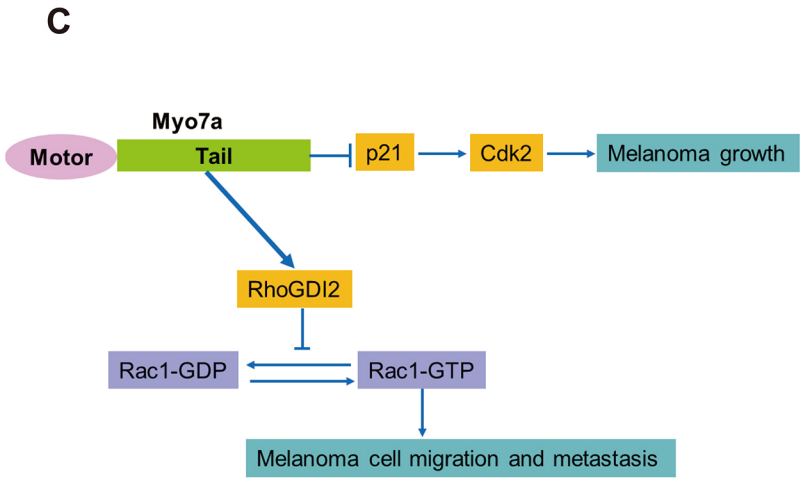

Fig. 7. Myo7a expression is increased in human melanomas. (A) Myo7a expression both in normal and melanoma tissues was determined by immunohistochemistry. (A1) Myo7a expression was detected in pancreas (negative tissue). (A2) Myo7a expression was detected in the tumor tissues (positive tissue), which originated from subcutaneous injection of A375 cells with stable overexpression of Myo7a. (B1) Myo7a was detected in the epidermis of normal skin. B2 shows a magnified view of the boxed area. (C1) Myo7a was detected in the dermis of normal skin. C2 shows a magnified view of the boxed area. (D1,E1,F1) Myo7a was detected in the human melanomas from three different patients, respectively. D2, E2 and F2 show a magnified view of the boxed area. (B) Statistics of Myosin 7a expression in Riker Melanoma were obtained from Oncomine data base. The box represents the 25–75th percentiles, and the median is indicated. The whiskers show the 10th–90th percentiles. For cutaneous melanoma vs normal, P=0.016. (C) A model depicting the role of Myo7a in the regulation of tumor growth and metastasis. Myo7a, containing an N-terminal domain with motor activity and a C-terminal tail domain that is heavily involved in protein–protein interactions, inhibits the cell cycle inhibitor p21, which leads to the upregulation of cell cycle-controlling kinase Cdk2, and thereby promotes tumor growth. In addition, Myo7a upregulates RhoGDI2, which activates the GTPase Rac1 by promoting GTP binding and sequestering inactive Rac1 (Rac1-GDP), and thus promotes tumor cell migration and metastasis.

found that Myo7a was highly expressed in mouse B16 melanoma cells, which were derived from a skin melanoma in C57BL/6 mice.

In the present investigation, we identified that Myo7a modulated melanoma cell motility. This conclusion was supported by several lines of evidence. First, depletion of Myo7a in B16 cells inhibited cell migration and invasion *in vitro*. Second, overexpression of Myo7a in A375 cells promoted tumor cell migration and invasion *in vitro*. Third, depletion of Myo7a in B16 cells suppressed tumor

Journal of Cell Science (2018) 131, jcs209924. doi:10.1242/jcs.209924

metastasis in an experimental model of metastasis and overexpression of Myo7a in A375 cells had the opposite effect. Since invasion and metastasis are important characteristics of malignant tumors, these findings indicate that Myo7a plays essential roles in melanoma development.

Mechanistically, we found that Myo7a regulated tumor motility by modulating the expression of RhoGDI2. RhoGDI2 inhibits the dissociation of GDP and further regulates GTPase function, and Rho GTPases are well-established regulators of cell migration and are implicated in the process of tumor cell invasion and metastasis (Raftopoulou and Hall, 2004; Rathinam et al., 2011; Ridley, 2001). RhoGDI2 expression has been reported in a series of tumor types. Intriguingly, RhoGDI2 plays bipartite roles in tumor progression (Griner and Theodorescu, 2012). RhoGDI2 acts as a tumor suppressor in bladder cancer and suppresses experimental lung metastasis (Gildea et al., 2002). However, RhoGDI2 expression is positively correlated with tumor progression and metastasis in gastric tumors (Cho et al., 2009). RhoGDI2 also promotes tumor growth, invasion and metastasis in ovarian carcinoma (Stevens et al., 2011) and in breast cancer (Gu et al., 2008; Zhang et al., 2009; Zhang and Zhang, 2006). It has been reported that RhoGDI2 suppresses anchorage-independent growth in melanoma B16 cells (Wang et al., 2011). In our study, we demonstrated that depletion of Myo7a inhibited melanoma cell motility by downregulating expression of RhoGDI2. Previous studies have suggested that RhoGDI2 inhibits tumor metastasis in bladder cancer but does not affect tumor cell growth or colony formation *in vitro*, or tumorigenesis *in vivo* (Gildea et al., 2002). Although RhoGDI2 mediates the metastatic processes of melanoma, understanding the underlying mechanisms requires further investigation. Furthermore, we examined the activation status of the Rho family of small GTPases, Rac1 and Cdc42. We found that knockdown of Myo7a resulted in significant decrease in Rac1 activation while not affecting the activation of Cdc42 (data not shown).

In our study, knockdown of Myo7a strikingly diminished cell proliferation *in vitro* and tumor growth *in vivo*, and vice versa. Gene expression profiling via RNA-seq revealed changes in gene expression of certain cell cycle-related genes, including p21 and Cdk2. It is known that p21, a Cdk inhibitor, inhibits Cdk2 and plays critical roles in the regulation of the G1 to S phase transition during the cell cycle (Waldman et al., 1995). Taken together, our findings suggest that Myo7a inhibits p21, which raises the level of Cdk2 and thereby promotes tumor growth, and that Myo7a also upregulates RhoGDI2 to promote tumor cell migration and metastasis (Fig. 7C). However, further investigation is required to pinpoint the mechanisms of Myo7a-regulated p21 expression.

In conclusion, we identified that Myo7a is able to function in non-specialized cells by demonstrating that Myo7a regulates melanoma proliferation, migration, invasion and metastasis via control of p21 and RhoGDI2 expression, which expands our current knowledge concerning Myo7a. Enhanced expression of Myo7a in human melanoma suggests an important role of Myo7a in the regulation of melanoma progression. Thus, Myo7a may be a candidate therapeutic target in human melanoma.

MATERIALS AND METHODS

Animals and cell lines

Female BALB/c nude mice and C57BL/6 mice that were 4–6 weeks old were purchased from the Animal Department of Peking University Health Science Center with approval of the Animal Care and Use Committee of Peking University Health Science Center (Permit Number: LA2011-73). Cell lines used in the present investigation were purchased from Cell Lines Collection Center of China (Beijing, PRC). Human melanoma cells A375 and M21, human breast cancer cells MCF-7 and MDA-MB-231, human lung cancer cells H1299, human cervix cancer cells HeLa and human colon cancer cells SW480 were cultured in Dulbecco's modified Eagle's medium (DMEM; Invitrogen, Carlsbad, CA) and mouse melanoma cells B16, human melanoma cells Mel57, WM983a, WM266-4 and WM1205 were cultured in RPMI 1640 (Invitrogen, Carlsbad, CA). Cell culture media were supplemented with 10% fetal bovine serum (FBS) (Invitrogen, Carlsbad, CA), 100 IU/ml penicillin and 100 µg/ml streptomycin. The cells were cultured at 37°C with 5% CO_2 in a humidified incubator.

RNA interference

Cells were plated in six-well plates and transfected with Myo7a siRNA, p21 siRNA, RhoGDI2 siRNA or control siRNA (QIAGEN, Hilden, Germany) at a final concentration of 100 nM using Lipofectamine RNAiMAX (Invitrogen, Carlsbad, CA). Sequences of RNAi oligonucleotides were as follows: Myo7a siRNA1, 5′-CAGAGTCATTC-TCCTCCAGAA-3′; Myo7a siRNA2, 5′-CCAGGTGTTCTTCATGAAG-AA-3′; p21 siRNA1, 5′-AGACCAGCCUGACAGAUUU-3′; p21 siRNA2, 5′-AACGGUGGAACUUUGACUUCG-3′; RhoGDI2 siRNA, 5′-GGAT-GACGAGAGTCTAACCAA-3′; control siRNA, 5′-CGAGUGGUCUAG-UUGAGAA-3′. Myo7a siRNA2 with higher knockdown efficiency was chosen to generate Myo7a shRNA. One pair of oligonucleotides was synthesized by Invitrogen. The forward oligonucleotide sequence was 5′-GATCCCCCCAGGTGTTCTTCATGAAGAATTCAAGAGATTCTTCA-TGAAGAACACCTGGTTTTTA-3′ and the reverse oligonucleotide sequence was 5′-AGCTTAAAAACCAGGTGTTCTTCATGAAGAATC-TCTTGAATTCTTCATGAAGAACACCTGGGGG-3′. The oligonucleotides were annealed and inserted into pSUPER vector to produce Myo7a shRNA, and the recombinant vector was verified by DNA sequencing.

Establishment of stable cell lines

B16 cells were transfected with control shRNA or Myo7a shRNA, and then were selected by 800 µg/ml G418 (Gibco, CA) for 3–4 weeks to establish stable clones. A375 cells were transfected with Flag or Flag-tagged Myo7a, which were also selected by 800 µg/ml G418 for 3–4 weeks to establish stable clones.

Western blot analysis

Cells lysates were prepared using PBSTDS lysis buffer containing cocktail protease inhibitor (Boehringer Mannheim, Mannheim, Germany). Proteins were denatured at 95°C for 5 min and then separated by SDS-PAGE. Separated proteins were transferred onto PVDF membrane (Millipore, Billerica, MA) following blocking with 5% milk in Tris-buffered saline (TBS) containing 1% Tween-20 for 1 h and incubated with primary antibodies overnight at 4°C. Primary antibodies used were: rabbit anti-Myo7a ab3481, Abcam, 1:1000; mouse anti-RhoGDI2, sc-376473, Santa Cruz Biotechnology, 1:200; mouse anti-p21, sc-6246, Santa Cruz Biotechnology, 1:500; rabbit anti-Rac1, #2465, Cell Signaling Technology, 1:1000; mouse anti-Cdc42, sc-8401, Santa Cruz Biotechnology, 1:500 and mouse anti-β-actin, sc-47778, Santa Cruz Biotechnology, 1:1000. All horseradish peroxidase (HRP)-coupled secondary antibodies (JIR) were used at 1:5000 dilution. The signal was detected using a chemiluminescence detection kit (Pierce, Rockford, IL).

WST-1 proliferation assay

Stable clones were seeded in 96-well plates at a density of 2000 cells per well and cultured for 5 days. 100 µl of 10% WST-1 was added to each well after removal of the growth medium. Then the cells were incubated for 1 h at 37°C, and the absorbance was measured at a wavelength of 450 nm on a microplate reader (Bio-Rad). Wells without cells were used as blank control and samples were analyzed in triplicate.

Colony formation assay

The colony formation assay in soft agar was carried out in a six-well plate. First, the basal layer was made by mixing 1.2% agarose (Invitrogen) and equivalent volume of 2× medium with 20% FBS. Then the stable cells were

Journal of Cell Science (2018) 131, jcs209924. doi:10.1242/jcs.209924

harvested and suspended in medium containing 0.3% agarose and plated over the basal layer in triplicate at a density of 5000 cells per well. After 2–3 weeks, cells were stained with 0.1% Crystal Violet when colonies were visible by the naked eye. The ability of colony formation was calculated by determining the total number of colonies per well.

Transplantation tumor experiment

The stable B16 Myo7a shRNA cells and the controls were trypsinized and washed twice with PBS and suspended in serum-free RPMI 1640. For implantations, six C57BL/6 mice were injected subcutaneously with 10^5 cells at both sides of the back, with one side being injected with control cells and the other with Myo7a knockdown cells. In gain-of-function experiments, by contrast, 10^6 A375 Flag–Myo7a and control cells were injected subcutaneously into the two sides on the back of the nude mice. Once tumors were observed, the tumor volumes were measured every other day and calculated using the formula: $(\text{length})\times(\text{width})^2\times(\pi/6)$. About 2 weeks later (4 weeks for nude mice), mice were killed when the biggest tumor reached 1 cm in diameter and then tumors were removed.

In vitro wound healing assay

At 48 h post transfection with siRNA, cells were serum-starved overnight. Then a confluent cell monolayer was scratched by a sterile 200 µl pipette tip and the wounded monolayer was washed twice to remove non-adherent cells. Images were photographed at 0 h after wounding and at regular intervals during cell migration to close the wound. For stable clones, cells were seeded into six-well plates and the wound healing assay was performed in the same way.

In vitro transwell assay

Stable cells were resuspended in medium containing 1% FBS at 10^6 cells/ml, and 100 µl of cell suspension was placed in the upper chamber (pore size of 8 µm, Costar, Corning, NY) [for invasion assays, 2 mg/ml Matrigel (BD Bioscience) was pre-coated]. Medium supplemented with 20% FBS was added to the bottom wells of the chambers. Samples were prepared in triplicate. After incubation for 5 h (for invasion assay, 48 h incubation) at 37°C, the cells on the upper side of the filters were gently removed using cotton swabs. Filters were fixed in 4% paraformaldehyde and stained with 0.1% Crystal Violet. Twelve microscopic fields were randomly chosen for analyses.

Time-lapse microscopy

The random motility of B16 cells was monitored by using time-lapse confocal microscopy (Carl Zeiss LSM780, Germany) as previously described (An et al., 2010). Briefly, B16 stably transfected with Myo7a shRNA and control shRNA were seeded in 60 mm dishes incubated at 37°C for 6 h and transferred to the microscope for imaging. Cells were maintained during imaging in an incubator with humidified air (95%) and 5% CO_2 at 37°C. A total of 15 observation fields were randomly selected with two cells in each field, and time-lapse imaging was performed for 17 h using a 10× dry objective with an interval of 30 min. The obtained images were converted to movie files by using ZEN software. Cell tracking was performed with ImageJ software, and the graph was created using GraphPad Prism 5.

Tail vein metastasis assay

Twelve C57BL/6 mice were randomly divided into two groups. Approximately 10^5 B16 Myo7a shRNA cells or control cells suspended in 100 µl serum-free medium were injected via the tail vein, respectively. After 14 days, mice in each group were killed, the lungs, kidneys and femurs were removed and photographed, and histochemical analysis was performed after fixation in Bouin's solution overnight.

The BALB/c nude mice were randomly divided into two groups consisting of six mice each. The mice were injected intravenously with 2×10^6 A375 cells overexpressing Myo7a or control vector, which were suspended in 100 µl of serum-free medium, through tail vein. After 30 days, the mice were killed, and the lungs were resected and histochemically analyzed.

RT-qPCR

Total RNA was extracted from the cells by using Trizol reagent (Invitrogen). Approximately 2 µg of RNA was used for the reverse transcription reaction with MMLV Reverse Transcriptase (Promega, CA). Real-time qPCR was performed by using SYBR Green mix (Applied Biosystems, CA) with the PCR conditions: 95°C for 3 min; 95°C for 20 s, 60°C for 1 min, for 40 cycles. The following primers were used for PCR: mouse Myo7a forward primer, 5′-ATCCTCCTGCCTCATGTTCAG-3′ and reverse primer, 5′-CGGGGAAGTAGACCTTGTGGA-3′; human Myo7a forward primer, 5′-GCAGCACTCGTGGATTGAG-3′ and reverse primer, 5′-TGTACTTTCCGAAACGGCTTG-3′; mouse MMP9 forward primer, 5′-CGAACTTCGACACTGACAAGAAGT-3′ and reverse primer, 5′-GCACGCTGGAATGATCTAAGC-3′; mouse RhoGDI2 forward primer, 5′-ATGACGGAGAAGGATGCACAG-3′ and reverse primer, 5′-CTCCCAGCAGTGTTTTCTTGTA-3′; mouse p21 forward primer, 5′-CCTGGTGATGTCCGACCTG-3′ and reverse primer, 5′-CCATGAGCGC-ATCGCAATC-3′; mouse Cdk2 forward primer, 5′-CCTGCTTATCAATG-CAGAGGG-3′ and reverse primer, 5′-TGCGGGTCACCATTTCAGC-3′; mouse GAPDH forward primer, 5′-GGCAAAGTGGAGATTGTTGC-3′ and reverse primer, 5′-AATTTGCCGTGAGTGGAGTC-3′; human β-Actin forward primer, 5′-CCTCGCCTTTGCCGATCCG-3′ and reverse primer, 5′-GCCGGAGCCGTTGTCGACG-3′. Samples were analyzed in triplicate and experiments were repeated three times.

Cell cycle analysis

The cell cycle distribution of cells was analyzed by flow cytometry assay following propidium iodide (PI) staining. Briefly, when the cells were ∼80% confluent, they were harvested and fixed in 0.5 ml cold 70% ethanol at −20°C overnight. The cells were then treated with 100 mg/ml of DNase-free RNase (Qiagen) and incubated for 30 min at 37°C. Before detection, PI (50 mg/ml; Sigma-Aldrich) was added directly to the cell suspension. Stained cells were subjected to fluorescence-activated cell sorting (FACS) analysis with a flow cytometer (FACSCalibur, BD Biosciences).

RNA sequencing

RNA sequencing was performed as described by De Bellis et al. (2014). In brief, total RNA was isolated by using Trizol (Invitrogen) according to the manufacturer's recommendations. Complementary DNA first and DscDNA synthesis was then performed by following supplier's instructions (Invitrogen). Cluster generation and sequencing-by-synthesis (36 bp) were performed by using the Illumina Hiseq2000 sequencing system according to standard protocols (Illumina). The gene expression values were obtained using Genomatix (www.genomatix.de) software. GO and Pathway analysis were performed using Panther (http://www.pantherdb.org).

Two-dimensional gel electrophoresis

Stable cells were harvested at 80% confluence and then were washed three times with PBS and homogenized on ice in lysis buffer containing 7 M urea, 2 M thiourea, 4% CHAPS, 65 mM dithiothreitol (DTT), 2 mM EDTA, 0.2% Bio-Lyte and protease inhibitor cocktail. After centrifugation at 17,500 ***g*** for 1 h, the supernatant was collected and the protein concentration was determined by the Bradford method. Approximately 200 µg protein was dissolved in rehydration buffer and loaded onto IPG strips (17 cm, pH 3-10, Bio-Rad). Isoelectric focusing was performed at 250 V for 30 min, followed by an increase in voltage to 10,000 V within 5 h, and this was maintained at 10,000 V until 60,000 volt hours were attained. Strips were placed in equilibration buffer (6 M urea, 2% SDS, 20% glycerol, 375 mM Tris-HCl pH 8.8) containing 2% DTT and shaken slowly for 15 min, then transferred to equilibration buffer containing 2.5% iodoacetamide and shaken for an additional 15 min. The strips were then transferred to 12% SDS polyacrylamide gels for separation in the second dimension. Proteins were visualized by silver staining, and the images were scanned and analyzed with PDQuest software, which was obtained from Bio-Rad. The differentially expressed spots were excised and verified by mass spectrometry (MS).

GST pulldown assays

Affinity precipitation with GST–PBD was performed using an assay as previously described by Zhang et al. (2010). In brief, glutathione–Sepharose beads (Amersham Pharmacia Biotech) were used to capture the GST fusion proteins and the interacting proteins. Cells lysates were prepared using PBSTDS lysis buffer (0.01 M PBS, 1% Triton X-100, 5 g/l Sodium deoxycholate, 1 g/l SDS and 1 mM EDTA) containing cocktail protease

inhibitor (Boehringer Mannheim, Mannheim, Germany). Equal amounts of protein supernatants were incubated at 4°C with GST–PAK1-CD fusion protein-coated glutathione–Sepharose beads overnight. The beads were washed, and the bound proteins were released by heat denaturing in protein loading buffer. Samples were then separated by 15% SDS-PAGE and detected by immunoblotting with antibodies against Rac1 (#2465, Cell Signaling Technology, 1:1000) and Cdc42 (sc-8401, Santa Cruz Biotechnology, 1:500).

Tissue samples and immunohistochemistry

Surgically removed melanoma tissues were collected from 15 patients at Peking University Cancer Hospital and Institute (Beijing, China); adjacent normal tissues used as the control. The experiments were approved by the Ethics Committee of Peking University Cancer Hospital and informed consent was obtained from all subjects.

Immunohistochemical staining for protein expression was performed on tissue sections. Briefly, sections were deparaffinized with xylene, followed by rehydration in ethanol. Sections were incubated overnight at 4°C with rabbit anti-Myo7a antibody (ab3481, Abcam, 1:100), and then incubated for 30 min with secondary antibodies (Dako, Carpinteria, CA). The immunostaining was examined with an Olympus BX51 microscope (Olympus, Tokyo, Japan).

Statistical analysis

All experiments were repeated three times, and data are presented as means± s.d. Statistical analyses were conducted using Graphpad Prism 5 (https://www.graphpad.com/scientific-software/prism/). A paired Student's *t*-test was used for comparison of tumor weight between the two groups, while an unpaired *t*-test was performed for other intergroup comparisons. $*P<0.05$; $**P<0.01$; $***P<0.001$.

Competing interests

The authors declare no competing or financial interests.

Author contributions

Conceptualization: H.Z.; Methodology: Y.L., X.W., L.G., X.H.; Software: Y.L., X.W., L.G., D.L.; Validation: Y.L., X.W., S.X., D.L.; Formal analysis: Y.L.; Investigation: Y.L., X.W., L.G., Y.Y., D.L., X.H.; Resources: X.W., J.Z., Y.K., J.G.; Data curation: Y.L., X.W., J.Z.; Writing - original draft: Y.L.; Writing - review & editing: X.W.; Visualization: X.W.; Supervision: H.Z.; Project administration: H.Z.; Funding acquisition: H.Z.

Funding

This study was supported by grants from the Ministry of Science and Technology of China (2016YFC1302103 and 2015CB553906), the National Natural Science Foundation of China (81230051, 30830048, 31170711, 81321003 and 81670626); and Beijing Municipal Natural Science Foundation (7120002 and 7171005), the 111 Project of the Ministry of Education, Peking University grants (BMU20120314 and BMU20130364), and a Leading Academic Discipline Project of Beijing Education Bureau to H.Z.

Supplementary information

Supplementary information available online at
http://jcs.biologists.org/lookup/doi/10.1242/jcs.209924.supplemental

References

An, Z., Dobra, K., Lock, J. G., Strömblad, S., Hjerpe, A. and Zhang, H. (2010). Kindlin-2 is expressed in malignant mesothelioma and is required for tumor cell adhesion and migration. *Int. J. Cancer* **127**, 1999-2008.

Arjonen, A., Kaukonen, R., Mattila, E., Rouhi, P., Högnäs, G., Sihto, H., Miller, B. W., Morton, J. P., Bucher, E., Taimen, P. et al. (2014). Mutant p53-associated myosin-X upregulation promotes breast cancer invasion and metastasis. *J. Clin. Invest.* **124**, 1069-1082.

Berg, J. S., Powell, B. C. and Cheney, R. E. (2001). A millennial myosin census. *Mol. Biol. Cell* **12**, 780-794.

Cho, H. J., Baek, K. E., Park, S.-M., Kim, I.-K., Choi, Y.-L., Cho, H.-J., Nam, I.-K., Hwang, E. M., Park, J.-Y., Han, J. Y., et al. (2009). RhoGDI2 expression is associated with tumor growth and malignant progression of gastric cancer. *Clin. Cancer Res.* **15**, 2612-2619.

De Bellis, F., Carafa, V., Conte, M., Rotili, D., Petraglia, F., Matarese, F., Francoijs, K.-J., Ablain, J., Valente, S., Castellano, R. et al. (2014). Context-selective death of acute myeloid leukemia cells triggered by the novel hybrid retinoid-HDAC inhibitor MC2392. *Cancer Res.* **74**, 2328-2339.

Fernandez, L. P., Milne, R. L., Pita, G., Floristan, U., Sendagorta, E., Feito, M., Avilés, J. A., Martin-Gonzalez, M., Lázaro, P., Benítez, J. et al. (2009). Pigmentation-related genes and their implication in malignant melanoma susceptibility. *Exp. Dermatol.* **18**, 634-642.

Foth, B. J., Goedecke, M. C. and Soldati, D. (2006). New insights into myosin evolution and classification. *Proc. Natl. Acad. Sci. USA* **103**, 3681-3686.

Frolenkov, G. I., Belyantseva, I. A., Friedman, T. B. and Griffith, A. J. (2004). Genetic insights into the morphogenesis of inner ear hair cells. *Nat. Rev. Genet.* **5**, 489-498.

Futter, C. E. (2006). The molecular regulation of organelle transport in mammalian retinal pigment epithelial cells. *Pigment Cell Res.* **19**, 104-111.

Futter, C. E., Ramalho, J. S., Jaissle, G. B., Seeliger, M. W. and Seabra, M. C. (2004). The role of Rab27a in the regulation of melanosome distribution within retinal pigment epithelial cells. *Mol. Biol. Cell* **15**, 2264-2275.

Gautreau, A., Louvard, D. and Arpin, M. (2002). ERM proteins and NF2 tumor suppressor: the Yin and Yang of cortical actin organization and cell growth signaling. *Curr. Opin. Cell Biol.* **14**, 104-109.

Gibson, F., Walsh, J., Mburu, P., Varela, A., Brown, K. A., Antonio, M., Beisel, K. W., Steel, K. P. and Brown, S. D. M. (1995). A type VII myosin encoded by the mouse deafness gene shaker-1. *Nature* **374**, 62-64.

Gildea, J. J., Seraj, M. J., Oxford, G., Harding, M. A., Hampton, G. M., Moskaluk, C. A., Frierson, H. F., Conaway, M. R. and Theodorescu, D. (2002). RhoGDI2 is an invasion and metastasis suppressor gene in human cancer. *Cancer Res.* **62**, 6418-6423.

Griner, E. M. and Theodorescu, D. (2012). The faces and friends of RhoGDI2. *Cancer Metastasis Rev.* **31**, 519-528.

Gu, Y., Zhang, J., Mi, W., Yang, J., Han, F., Lu, X. and Yu, W. (2008). Silencing of GM3 synthase suppresses lung metastasis of murine breast cancer cells. *Breast Cancer Res.* **10**, R1.

Hasson, T., Heintzelman, M. B., Santos-Sacchi, J., Corey, D. P. and Mooseker, M. S. (1995). Expression in cochlea and retina of myosin VIIa, the gene product defective in Usher syndrome type 1B. *Proc. Natl. Acad. Sci. USA* **92**, 9815-9819.

Hirano, Y., Hatano, T., Takahashi, A., Toriyama, M., Inagaki, N. and Hakoshima, T. (2011). Structural basis of cargo recognition by the myosin-X MyTH4-FERM domain. *EMBO J.* **30**, 2734-2747.

Jemal, A., Simard, E. P., Dorell, C., Noone, A.-M., Markowitz, L. E., Kohler, B., Eheman, C., Saraiya, M., Bandi, P., Saslow, D. et al. (2013). Annual Report to the Nation on the Status of Cancer, 1975-2009, featuring the burden and trends in human papillomavirus (HPV)-associated cancers and HPV vaccination coverage levels. *J. Natl. Cancer Inst.* **105**, 175-201.

Kros, C. J., Marcotti, W., van Netten, S. M., Self, T. J., Libby, R. T., Brown, S. D. M., Richardson, G. P. and Steel, K. P. (2002). Reduced climbing and increased slipping adaptation in cochlear hair cells of mice with Myo7a mutations. *Nat. Neurosci.* **5**, 41-47.

Liu, X.-Z., Walsh, J., Mburu, P., Kendrick-Jones, J., Cope, M. J. T. V., Steel, K. P. and Brown, S. D. M. (1997a). Mutations in the myosin VIIA gene cause non-syndromic recessive deafness. *Nat. Genet.* **16**, 188-190.

Liu, X.-Z., Walsh, J., Tamagawa, Y., Kitamura, K., Nishizawa, M., Steel, K. P. and Brown, S. D. M. (1997b). Autosomal dominant non-syndromic deafness caused by a mutation in the myosin VIIA gene. *Nat. Genet.* **17**, 268-269.

Liu, X., Udovichenko, I. P., Brown, S. D., Steel, K. P. and Williams, D. S. (1999). Myosin VIIa participates in opsin transport through the photoreceptor cilium. *J. Neurosci.* **19**, 6267-6274.

Liu, Y., Guan, L., Zhan, J., Lu, D., Wan, J. and Zhang, H. (2014). FERM domain-containing unconventional myosin VIIA interacts with integrin beta5 subunit and regulates alphavbeta5-mediated cell adhesion and migration. *FEBS Lett.* **588**, 2859-2866.

Lopes, V. S., Ramalho, J. S., Owen, D. M., Karl, M. O., Strauss, O., Futter, C. E. and Seabra, M. C. (2007). The ternary Rab27a-Myrip-Myosin VIIa complex regulates melanosome motility in the retinal pigment epithelium. *Traffic* **8**, 486-499.

Marsh Durban, V., Deuker, M. M., Bosenberg, M. W., Phillips, W. and McMahon, M. (2013). Differential AKT dependency displayed by mouse models of BRAFV600E-initiated melanoma. *J. Clin. Invest.* **123**, 5104-5118.

Mburu, P., Liu, X. Z., Walsh, J., Saw, D., Jr, Cope, M. J., Gibson, F., Kendrick-Jones, J., Steel, K. P. and Brown, S. D. (1997). Mutation analysis of the mouse myosin VIIA deafness gene. *Genes Funct.* **1**, 191-203.

Raftopoulou, M. and Hall, A. (2004). Cell migration: Rho GTPases lead the way. *Dev. Biol.* **265**, 23-32.

Rathinam, R., Berrier, A. and Alahari, S. K. (2011). Role of Rho GTPases and their regulators in cancer progression. *Front. Biosci.* **16**, 2561-2571.

Richards, T. A. and Cavalier-Smith, T. (2005). Myosin domain evolution and the primary divergence of eukaryotes. *Nature* **436**, 1113-1118.

Ridley, A. J. (2001). Rho GTPases and cell migration. *J. Cell Sci.* **114**, 2713-2722.

Rzadzinska, A. K., Nevalainen, E. M., Prosser, H. M., Lappalainen, P. and Steel, K. P. (2009). MyosinVIIa interacts with Twinfilin-2 at the tips of mechanosensory stereocilia in the inner ear. *PLoS ONE* **4**, e7097.

Soni, L. E., Warren, C. M., Bucci, C., Orten, D. J. and Hasson, T. (2005). The unconventional myosin-VIIa associates with lysosomes. *Cell Motil. Cytoskeleton* **62**, 13-26.

Stevens, E. V., Banet, N., Onesto, C., Plachco, A., Alan, J. K., Nikolaishvili-Feinberg, N., Midkiff, B. R., Kuan, P. F., Liu, J., Miller, C. R. et al. (2011). RhoGDI2 antagonizes ovarian carcinoma growth, invasion and metastasis. *Small GTPases* **2**, 202-210.

Tamagawa, Y., Ishikawa, K., Ishida, T., Kitamura, K., Makino, S., Tsuru, T. and Ichimura, K. (2002). Phenotype of DFNA11: a nonsyndromic hearing loss caused by a myosin VIIA mutation. *Laryngoscope* **112**, 292-297.

Waldman, T., Kinzler, K. W. and Vogelstein, B. (1995). p21 is necessary for the p53-mediated G1 arrest in human cancer cells. *Cancer Res.* **55**, 5187-5190.

Wang, P., Xu, S., Wang, Y., Wu, P., Zhang, J., Sato, T., Yamagata, S. and Yamagata, T. (2011). GM3 suppresses anchorage-independent growth via Rho GDP dissociation inhibitor beta in melanoma B16 cells. *Cancer Sci.* **102**, 1476-1485.

Wang, T., Pei, X., Zhan, J., Hu, J., Yu, Y. and Zhang, H. (2012). FERM-containing protein FRMD5 is a p120-catenin interacting protein that regulates tumor progression. *FEBS Lett.* **586**, 3044-3050.

Weil, D., Blanchard, S., Kaplan, J., Guilford, P., Gibson, F., Walsh, J., Mburu, P., Varela, A., Levilliers, J., Weston, M. D. et al. (1995). Defective myosin VIIA gene responsible for Usher syndrome type 1B. *Nature* **374**, 60-61.

Weil, D., Küssel, P., Blanchard, S., Lévy, G., Levi-Acobas, F., Drira, M., Ayadi, H. and Petit, C. (1997). The autosomal recessive isolated deafness, DFNB2, and the Usher 1B syndrome are allelic defects of the myosin-VIIA gene. *Nat. Genet.* **16**, 191-193.

Wolfrum, U., Liu, X., Schmitt, A., Udovichenko, I. P. and Williams, D. S. (1998). Myosin VIIa as a common component of cilia and microvilli. *Cell Motil. Cytoskeleton* **40**, 261-271.

Woolner, S. and Bement, W. M. (2009). Unconventional myosins acting unconventionally. *Trends Cell Biol.* **19**, 245-252.

Zhang, Y. and Zhang, B. (2006). D4-GDI, a Rho GTPase regulator, promotes breast cancer cell invasiveness. *Cancer Res.* **66**, 5592-5598.

Zhang, H., Berg, J. S., Li, Z., Wang, Y., Lång, P., Sousa, A. D., Bhaskar, A., Cheney, R. E. and Strömblad, S. (2004). Myosin-X provides a motor-based link between integrins and the cytoskeleton. *Nat. Cell Biol.* **6**, 523-531.

Zhang, Y., Rivera Rosado, L. A., Moon, S. Y. and Zhang, B. (2009). Silencing of D4-GDI inhibits growth and invasive behavior in MDA-MB-231 cells by activation of Rac-dependent p38 and JNK signaling. *J. Biol. Chem.* **284**, 12956-12965.

Zhang, Y., Gong, L.-H., Zhang, H.-Q., Du, Q., You, J.-F., Tian, X.-X. and Fang, W.-G. (2010). Extracellular ATP enhances in vitro invasion of prostate cancer cells by activating Rho GTPase and upregulating MMPs expression. *Cancer Lett.* **293**, 189-197.